FEBS Letters 589 (2015) 2283–2289

FEBS Letters

journal homepage: www.FEBSLetters.org

High-resolution structures of the D-alanyl carrier protein (Dcp) DltC from *Bacillus subtilis* reveal equivalent conformations of *apo*- and *holo*-forms

Stephan Zimmermann [a,1,2], Sabrina Pfennig [a,3], Piotr Neumann [a,4], Huma Yonus [a], Ulrich Weininger [b,5], Michael Kovermann [b,6], Jochen Balbach [b], Milton T. Stubbs [a,*]

[a] Institut für Biochemie und Biotechnologie, Martin-Luther Universität Halle-Wittenberg, Kurt-Mothes Strasse 3, D-06120 Halle/Saale, Germany
[b] Institut für Physik, Martin-Luther-Universität Halle-Wittenberg, Betty-Heimann-Straße 7, D-06120 Halle/Saale, Germany

ARTICLE INFO

Article history:
Received 4 May 2015
Revised 2 July 2015
Accepted 7 July 2015
Available online 17 July 2015

Edited by Miguel De la Rosa

Keywords:
Carrier protein
Posttranslational modification
Structure
Dynamics
Lipoteichoic acid biosynthesis
Non-ribosomal peptide synthesis

ABSTRACT

D-Alanylation of lipoteichoic acids plays an important role in modulating the properties of Gram-positive bacteria cell walls. The D-alanyl carrier protein DltC from *Bacillus subtilis* has been solved in *apo*- and two cofactor-modified *holo*-forms, whereby the entire phosphopantetheine moiety is defined in one. The atomic resolution of the *apo*-structure allows delineation of alternative conformations within the hydrophobic core of the 78 residue four helix bundle. In contrast to previous reports for a peptidyl carrier protein from a non-ribosomal peptide synthetase, no obvious structural differences between *apo*- and *holo*-DltC forms are observed. Solution NMR spectroscopy confirms these findings and demonstrates in addition that the two forms exhibit similar backbone dynamics on the ps–ns and ms timescales.

1. Introduction

Modification of lipoteichoic acids influences the net charge of the cell wall in Gram-positive bacteria, and as such plays a role in adaptation to changing environmental conditions [1]. The most common modification, the covalent linkage of a D-alanine, decreases susceptibility to cationic antimicrobial peptides, glycopeptides and lytic enzymes produced by neutrophils [2–4]. D-alanylation is accomplished by proteins of the *dlt-operon* [5]; the free amino acid D-alanine is activated by the enzyme DltA in an ATP consuming reaction and transferred to the free thiol group of a 4′-phosphopantetheine (ppant) cofactor attached to the carrier protein DltC. The thioester-linked D-alanine is subsequently transported over the membrane to be incorporated in lipoteichoic acids by an as yet unknown mechanism.

DltC is closely related to the acyl and peptidyl carrier proteins (ACPs and PCPs, respectively) [6], which play crucial roles in the biosynthesis of fatty acids (FAs), polyketides (PKs) and non-ribosomal peptides (NRPs), respectively. ACPs and PCPs may be found as individual domains within large modular polypeptides (type I carrier proteins) or as stand-alone domains (type II carrier proteins). Despite diverse sequences and participation in a wide range of reactions, carrier proteins share a common four helix

Abbreviations: CP, carrier protein; Dcp, D-alanyl CP; ACP, acyl CP; PCP, peptidyl CP; ArCP, aryl CP; ppant, 4′-phosphopantetheine; FA, fatty acid; PK, polyketide; NRP, non-ribosomal peptide; SeMet, selenomethionine; rmsd, root mean square deviation

Author contributions: S.Z., S.P. and H.Y. expressed, prepared and crystallized apo- and *holo*-DltC; S.Z. and P.N. collected the diffraction data and solved the crystal structures; S.Z. and S.P. prepared labelled proteins for NMR measurements, which were performed, analysed and interpreted by U.W., M.K. and J.B.; S.Z., S.P. and M.T.S wrote the paper, which was discussed by all authors.

* Corresponding author. Fax: +49 345 55 27360.
E-mail address: stubbs@biochemtech.uni-halle.de (M.T. Stubbs).

[1] This paper is dedicated to the memory of our friend and colleague Dr. Stephan Zimmermann, whose sudden death so early in his scientific career has been a tragic loss to us all.

[2] Present address: Institute of Immunology & Infection Research, University of Edinburgh, King's Buildings, Ashworth Laboratories, West Mains Road, Edinburgh EH9 3JT, UK.
[3] Present address: Molecular Biology Unit, Adolf-Butenandt-Institut, Ludwig-Maximilians-Universität München, Schillerstr. 44, D-80336 Munich, Germany.
[4] Present address: Institut für Mikrobiologie und Genetik, Georg-August-Universität, Justus-von-Liebig-Weg 11, D-37077 Göttingen, Germany.
[5] Present address: Department of Biophysical Chemistry, Lund University, SE-22100 Lund, Sweden.
[6] Present address: Department of Chemistry, Umeå University, SE-90187 Umeå, Sweden.

http://dx.doi.org/10.1016/j.febslet.2015.07.008

bundle fold as well as the coenzyme A-derived posttranslational modification ppant, which is covalently attached to a conserved serine residue (Ser36 in DltC from *B. subtilis*) near the N-terminus of helix II by phosphopantetheinyl transferases such as the acyl carrier protein synthase (ACPS) or Sfp (surfactin synthase activating enzyme)-like enzymes (for PCPs). In the biosynthesis of FAs, PKs and NRPs, the growing product chain in each case becomes covalently bound to the cofactor thiol group of a corresponding carrier protein for transfer between the contributing catalytic centres within the molecular assembly line. Carrier proteins must therefore interact in a specific order with diverse enzymes (or domains) to direct correct product synthesis. With a size of around 80 amino acids, the surface available for potential interactions is obviously limited, raising questions as to how this can be accomplished.

Two theories in particular have been discussed in the literature for natural product assembly line synthesis [7]: (i) the enzymes interact directly with the substrate bound ppant cofactor, with the protein itself playing only a minor role (e.g. the *swinging arm* hypothesis in FA synthesis), or (ii) conformational changes upon cofactor/substrate attachment facilitate specific interactions with alternative binding partners (as suggested for NRP biosynthesis) [8,9]. ACPs, responsible for the exchange of growing acyl chains between active centers within the FA and PK synthetases, can accommodate intermediary acyl-chains with a size of up 10 carbon atoms [10] through burial within the hydrophobic core, accompanied by small rearrangements in secondary structure dominated by a repositioning of helix III [11,12]. A minor shift in helix III has also been reported prior to substrate loading in the actinorhodin PK synthase ACP upon charging *apo*-ACP to generate the *holo*-form [13,14].

Due to the more hydrophilic character of amino acid/peptide intermediates, it is unlikely that thiol-linked intermediates are buried in PCPs [15]. Although methodologies have recently been developed for the study of substrate loaded PCPs [16], no structures have been reported so far. On the other hand, major structural differences in solution have been claimed between the *apo*- and *holo*-forms of the type I peptidyl carrier protein TycC3-PCP (excised from the tyrocidine NRP synthase) [8]. Three distinct conformations were described: an A-form for *apo*-PCP in absence of the ppant cofactor, an H-form for *holo*-PCP in presence of the cofactor, and a so-called A/H-conformation adopted by both the *apo*- and *holo*-PCP, which corresponds to the typical four helix bundle architecture observed for other ACPs and PCPs and reported earlier for the TycC3-PCP [15]. The cofactor bearing helix II shows significantly altered orientations in the A, A/H and H conformations, with the A form reflecting the most flexible and expanded conformation and the H-form exhibiting an unfolded helix III. Based on these data, it has been suggested that the PCP phosphopantetheinyl transferase Sfp recognizes the A-conformation of the PCP [8], whereas the terminal thioesterase domain Srf-TE recognizes the H-form [9].

Although such inherent plasticity of the carrier protein provides an attractive model for an ordered trajectory from one active site to another, no such major structural rearrangements have been observed in any other carrier protein. Few comparative structural studies of PCPs in both their *apo*- and *holo*-forms have been reported. Crystal structure analyses of the aryl carrier protein (ArCP) from EntB of the enterobactin NRPS reveal the "A/H" conformation in both the *apo*- and *holo*-forms [17,18]. Recently, NMR structures of the excised terminal PCP from the teicoplanin NRPS also revealed the "A/H" conformation, with only subtle differences between *apo*- and *holo*-forms [19]. Thus the existence of the alternative "A-" and "H-" states has been called into question [20–22].

As the first steps in lipoteichoic acid modification exhibit features common to both fatty acid and non-ribosomal peptide synthesis, [23,24] we have investigated the structural properties of the D-alanyl carrier protein (Dcp) DltC from *B. subtilis*. Dcp is unusual for amino acid carrier proteins in that it can be charged by the *Escherichia coli* ACPS [6,25], and an NMR solution structure of *apo*-Dcp from *Lactobacillus rhamnosus* (*Lr*DltC) has been described [6]. Here we present a high resolution crystal structure of DltC in its *apo*-form, as well as the first crystal structures of a Type II PCP in *holo*-form. Complementing these results with NMR solution data, we show that DltC does not undergo any significant backbone rearrangements upon cofactor modification.

2. Experimental procedures

2.1. Gene cloning, mutation, expression and protein purification

DltC with a C-terminal His_6-tag was produced from the *B. subtilis dltC* gene cloned into the pQE-60 *E. coli* expression vector and transformed into *E. coli* BL21 (DE3) as described [25]. To mimic the *apo* form, Ser36 was mutated to alanine using the primers TTG CTT GAT GCT TTT GGA ACA GT (forward) and ACT GTT CCA AAA GCA TCA AGC AA (reverse) to yield DltC Ser36Ala. Cells were grown in LB-medium at 37 °C to an OD of 0.6 and expression induced with 1 mM IPTG. After 4 h expression at 37 °C, cells were harvested by centrifugation at 6 000 g for 20 min. The cell pellet was resuspended in 50 mM HEPES, 300 mM NaCl, 20 mM imidazole pH 7.8 and lysed by sonication. After centrifugation at 20 000×g for 20 min, the supernatant was applied to an affinity column (His-Trap, GE Healthcare) and eluted using a linear gradient up to 250 mM imidazole. DltC-containing fractions were pooled and further purified with a size exclusion chromatography column (Superdex 75 prep grade, GE Healthcare) using 50 mM HEPES, 300 mM NaCl, pH 7.8 as buffer. Expression and purification of wild type DltC resulted in both *apo*- and *holo*-DltC species in ratios between ca. 1:1 and 1:10; *holo*-DltC appeared as dimeric species under non-reducing conditions that dissociated readily in the presence of reducing agents. All steps were monitored by SDS–PAGE to analyze protein content and purity.

Selenomethionine (SeMet) labelled DltC Ser36Ala was produced by growing *E. coli* BL21 (DE3) in M9 minimal medium supplemented with lysine, phenylalanine, threonine, leucine, isoleucine, valine and selenomethionine, using the same growth-, induction- and expression-conditions as for the unlabeled protein. DltC for NMR-experiments was expressed using M9 minimal medium supplemented with ^{13}C-labeled glucose and ^{15}N-labeled $(NH_4)_2SO_4$. To ensure high purity and uniformity of the protein samples for NMR measurements, *holo*-DltC was expressed in *E. coli* BL21 (DE3) cells co-transformed with the pREP4 plasmid containing the gene *sfp* for the *B. subtilis* 4′-phosphopantetheinyl transferase Sfp; co-expression resulted almost exclusively in the *holo* form, as confirmed by mass spectrometry.

2.2. Crystallization, data collection and structure determination

Crystallization screening was carried out in 96-well plates (Greiner BioOne) and fine screening in 24-well plates (Qiagen EasyXtal). First crystals of *holo*-DltC (crystal form I, Supplementary Fig. 1) grew in 0.1 M sodium acetate, 0.2 M ammonium acetate, 30% PEG 4000, pH 5.7. Oscillation photographs were collected at the BESSY synchrotron (Berlin, Germany) on beam line BL14.1 at a wavelength of $\lambda = 0.9184$ Å and the data reduced using the XDS package [26] or MOSFLM and SCALA as implemented in CCP4 [27]. Crystals belonging to space group $P6_122$ ($a = b = 72.7$ Å, $c = 110.3$ Å, $\alpha = \beta = 90°$, $\gamma = 120°$) diffracted to 2.2 Å and contain two molecules in the asymmetric unit. A second crystal form (form II) was obtained in 95 mM sodium-citrate, 19% PEG 4000, 19%

2-propanol, 8% glycerol, pH 5.6. In house data were collected using CuKα radiation (λ = 1.5418 Å) on an RA Micro 007 rotating anode X-ray source equipped with an R Axis IV++ image plate detector, an X-Stream cryo-nitrogen stream and VarimaxTM Optics (Rigaku/MSC). The crystals diffracted to 1.8 Å, belong to space group $P6_522$ ($a = b = 49.2$ Å, $c = 146.3$ Å, $\alpha = \beta = 90°$, $\gamma = 120°$) and contain one molecule in the asymmetric unit.

As attempts to solve the structure of *holo*-DltC by molecular replacement using previously published NMR and X-ray structures of PCPs and ACPs (including that of *apo*-DltC from *L. rhamnosus* (*Lr*DltC or Dcp)) [6] proved unsuccessful in both crystal forms, SeMet MAD phasing was initiated. The SeMet-labeled Ser36Ala *apo*-DltC crystallized in 25% w/v PEG 3350, 100 mM bis–Tris, pH 5.5. The monoclinic crystals (space group $P2_1$, with $a = 34.5$ Å, $b = 37.2$ Å, $c = 37.7$ Å and $\alpha = \gamma = 90°$, $\beta = 114.8°$) diffracted at beam line BESSY-MX BL14.1 to 1.01 Å and contain one molecule in the asymmetric unit. Using data collected at wavelengths of 0.9798 Å (peak), 0.9799 Å (inflection) and 0.9184 Å (remote), the anomalous signal from the partially disordered N-terminal methionine Met1 was sufficient for phasing using the SHELX programme suite [28] navigated using hkl2map [29]. Automated model building was carried out using ARP/wARP [30] within CCP4, followed by cycles of manual rebuilding using Coot [31] and refinement using PHENIX [32] as implemented in the CCP4 program suite. The final electron density maps allowed modelling of all 78 DltC residues, together with those of the C-terminal Arg79-Ser80-His_6-tag. The resulting coordinates (after removal of the C-terminal tag residues) were used as template to obtain initial phases for *holo*-DltC in crystal forms I and II by molecular replacement using PHASER [33]. Crystal form I revealed density for all 78 DltC residues in both monomers, together with the phosphate of the bound ppant cofactor at Ser36. In addition, the complete ppant cofactor as well as the C-terminal expression tag was fully interpretable in crystal form II. Data collection and refinement statistics are given in Table 1.

3. ^{1}H-^{15}N NMR measurements

NMR measurements were performed in 100 mM HEPES pH 7.8, 150 mM NaCl, 3 mM TCEP and 10 mM $MgCl_2$ at 298 K. All buffers contained 10% (v/v) D_2O. Spectra were measured in a Bruker Avance III 800 spectrometer equipped with a TCI cryoprobe and a Bruker Avance III 600 spectrometer equipped with a QXI probe. ^{13}C/^{15}N labelled *holo*-DltC and ^{13}C/^{15}N Ser36Ala *apo*-DltC were used for peak assignments. The backbone resonances of 73 *apo*-DltC residues were assigned on the basis on HNCA, HNCACAB, HN(CO)CACB triple resonance spectra, although no resonances corresponding to Ala36 in *apo*-DltC could be identified. ^{1}H-^{15}N TROSY HSQC spectra of ^{15}N labelled DltC were recorded for conformational studies of *holo*-DltC and *apo*-DltC. As the *holo*-form of DltC shows no significant chemical shift changes, all assignments could be transferred from *apo*-DltC and were confirmed by triple resonance experiments. Two additional correlation peaks could be assigned to the ppant cofactor amides. Chemical shift differences $\Delta\omega^{all}$ between the *apo* and *holo* forms were calculated according to:

$$\Delta\omega^{all} = \sqrt{\left\{\frac{\left(^1H_{holo}-^1H_{apo}\right)^2 + \left(^{15}N_{holo}-^{15}N_{apo}\right)^2/25}{2}\right\}}$$

using the corresponding chemical shifts in the proton and nitrogen dimensions [34]. Steady-state {^{1}H}-^{15}N heteronuclear NOE experiments were recorded at $T = 298$ K and a magnetic field strength of 14.1 T in an interleaved manner by applying 600 saturation 120° pulses (each 5 ms long) to the proton channel. ^{15}N single quantum R_2 relaxation dispersion data were recorded at $T = 298$ K and a magnetic field strength of 14.1 T in a series of ^{1}H-^{15}N correlation spectra. The constant time relaxation delay was set to 40 ms to ensure that the peak intensity in the Carr–Purcell–Meiboom–Gill (CPMG) relaxation spectrum was about 50% of the intensity in the reference

Table 1
Data collection and refinement statistics for DltC crystal forms.

A. Data collection	*apo*-DltC (Ser36Ala)			*holo*-DltC form I form I	*holo*-DltC form II
Beamline	BESSY 14.1			BESSY 14.1	In-house
Wavelength λ (Å)	0.9184 (remote = native)	0.9799 (inflection)	0.97976 (peak)	0.9184	1.5418
Temperature (K)	100	100	100	100	100
Space group	$P2_1$			$P6_122$	$P6_522$
Molecules/asu	1			2	1
Unit cell constants					
a, *b*, *c* (Å)	34.58	34.53	34.52	72.68	49.21
	37.21	37.17	37.16	72.68	49.21
	37.69	37.69	37.68	110.30	146.26
α, β, γ (°)	90.00	90.00	90.00	90.00	90.00
	114.82	114.83	114.84	90.00	90.00
	90.00	90.00	90.00	120.00	120.00
Resolution range (Å)	100–1.01 (1.07–1.01)	100–2.8 (2.87–2.8)	100–2.81 (2.88–2.81)	62.94–2.2 (2.32–2.2)	40.93–1.95 (2.0–1.95)
No. unique reflections	40503 (2895)	3977 (309)	4006 (316)	9293 (1300)	8344 (1174)
Multiplicity	3.6 (3.4)	2.2 (2.2)	2.2 (2.2)	11.2 (11.5)	19.5 (19.8)
Completeness (%)	96.6 (94.4)	94.4 (96.6)	96.4 (99.1)	99.9 (100)	100 (100)
$I/\sigma I$	13.9 (2.5)	42.3 (38.4)	36.1 (33.3)	16.6 (3.8)	27.4 (6.0)
R_{meas} (%)	6.6 (66.6)	2.4 (2.5)	2.9 (2.8)	9.6 (80.6)	8.8 (56.0)
B. Refinement					
No. of residues (protein/cofactor/solvent)	709/0/137			1293/8/44	689/24/56
R_{cryst} (%)	11.9			20.9	19.0
R_{free} (%)	13.5			23.6	24.0
rmsd bond length (Å)	0.010			0.002	0.016
rmsd bond angles (°)	1.35			0.534	1.44
Mean *B* (Å^2)	14.58			38.76	32.55
Ramachandran plot (%)					
Preferred	98.5			96.1	94.8
Allowed	1.5			3.9	5.2
Disallowed	0			0	0
Pdb code	4bpf			4bpg	4bph

spectrum omitting the relaxation period [35]. All data were recorded using Topspin 2.1 (Bruker Biospin), processed with NMRPipe [36] and analysed with NMRView [37].

4. Results and discussion

Within the monoclinic crystal form, *apo*-DltC exhibits the four helix bundle typical of carrier proteins (Fig. 1), with a root mean square deviation (rmsd) in Cα positions of 1.44 Å to *apo-Lr*DltC (mean structure, 1hqb.pdb) [6]. Helices I (Asp2-Gln16), II (Asp35-Asp51) and IV (Thr66-Lys79), which each possess an "N-cap" residue (Asp2, Asp35 and Thr66, respectively) [38], are of similar length to each other with an up-down-down topology, forming a right handed helix bundle with the almost perpendicular short helix III (Pro55–Phe59) lying on top. The largest loop region between helices I and II is characterised by an additional helix I', comprised by residues Asp18-Asn23, as observed for *apo-Lr*DltC as well as ACP from *B. subtilis* [39]. Apart from a pronounced hydrophobic surface centred on helices II and III, which based on recent structural data is likely to be involved in interaction with the adenylation enzyme DltA [18,40], the protein surface is composed predominantly of polar (with an excess of negatively charged) residues.

The atomic resolution of the *apo*-DltC crystal structure allows reliable assignment of alternative conformations of core residue side chains (Fig. 1B), although this has no discernible effect on the positioning of backbone atoms and secondary structure

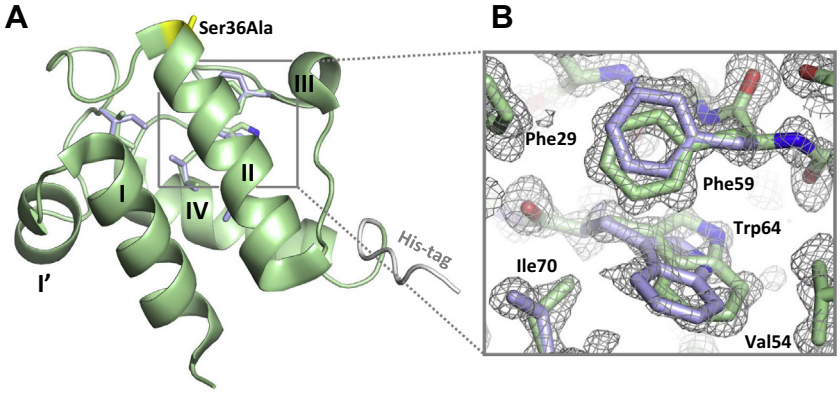

Fig. 1. 1.01 Å resolution structure of *apo*-DltC. (A) Overall fold reveals the typical four-helix (I, II, III and IV) bundle observed for other carrier proteins. The attachment site for the 4′-phosphopantetheinyl cofactor ppant (Ser36Ala, at the N-terminus of helix II) is coloured yellow. (B) Close up view of the final $2F_o–F_c$ electron density (contoured at 1σ), demonstrating major (green) and minor (blue) occupancy conformers within the hydrophobic core.

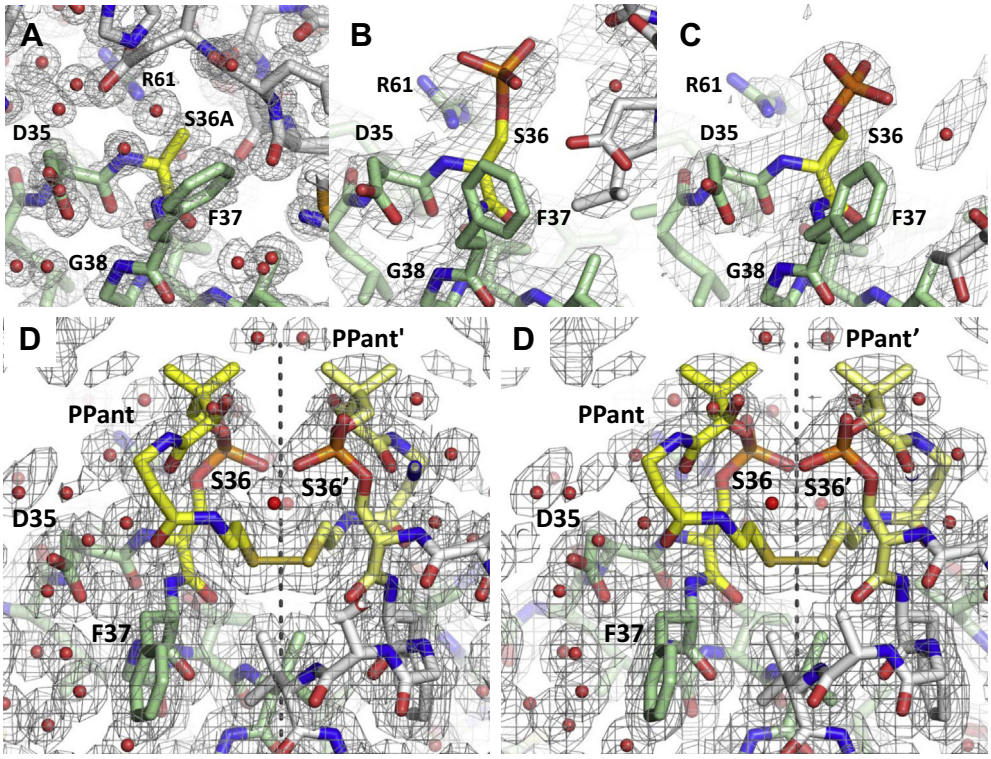

Fig. 2. Experimental $2F_o–F_c$ electron densities (contoured at 1σ) in the vicinity of the ppant attachment site Ser(Ala)36; carbon atoms of symmetry-related molecules depicted as white sticks. (A) *apo*-DltC; (B, C) *holo*-DltC monomers A/B respectively in crystal form I, showing density for the ppant phosphate moiety; the remainder of the prosthetic group is presumably disordered in both cases. (D) Stereo representation of the equivalent region in *holo*-DltC, crystal form II. Note the well-defined density for the cofactor, which is stabilized by forming a disulfide bond to the cofactor (light yellow) of a symmetry-related molecule.

elements. In particular, the partially surface exposed aromatic side chains of Trp64 and Phe59 can be refined in two distinct orientations, with a ratio of major:minor occupancies of ca. 2:1. On the other hand, NMR ^{1}H-^{15}N correlation spectra show only one distinct signal for the indole nitrogen of Trp64 (see below, Fig. 3A) and ^{15}N relaxation data obtained from R_2 relaxation dispersion experiments show no sign of millisecond dynamics. Within the NMR structure ensemble for *apo-Lr*DltC (1dv5.pdb) [6], the residue equivalent to Phe59 (Phe62) also demonstrates considerable positional variability, suggesting that this side chain is only weakly constrained in solution. In the crystal structure, the conformational diversity centred on Trp64/Phe59 extends to the neighbouring aliphatic side chains of residues Ile28, Ile46 and Ile70, which are completely buried within the protein core between helices II, III and IV.

Clear electron density corresponding to a phosphate moiety could be observed covalently linked to the side chain of Ser36 in both molecules of *holo*-DltC within the asymmetric unit of crystal form I (Fig. 2B, C). Superposition of the individual monomers on the *apo*-DltC structure yields rmsds for the Cα atoms of residues Met1 to Lys78 of 0.67 Å (monomer A)/0.72 Å (monomer B); monomers A and B differ by an rmsd of 0.31 Å. All residues of the core adopt the major occupancy conformation observed in the *apo*-form, although the absence of evidence for a minor conformation may be due to the lower diffraction limit of the *holo*-crystals. The Ser36-phosphate side chain of each monomer in the asymmetric unit adopts slightly different conformers (*gauche* (−) vs. *gauche* (+)); in both cases, the negative charge of the phosphate moiety is (at least in part) compensated by a close approach of the guanidinium function of Arg61, which itself enters into a planar stacking interaction [41] with the aromatic side chain of Phe29. No density is observed for the remainder of the ppant moiety, which we assume is flexible in the crystal lattice. In solution, the low values for the ppant amides in the {^{1}H}-^{15}N heteronuclear NOE experiments (see below, Fig. 3B) indicate high flexibility of the cofactor

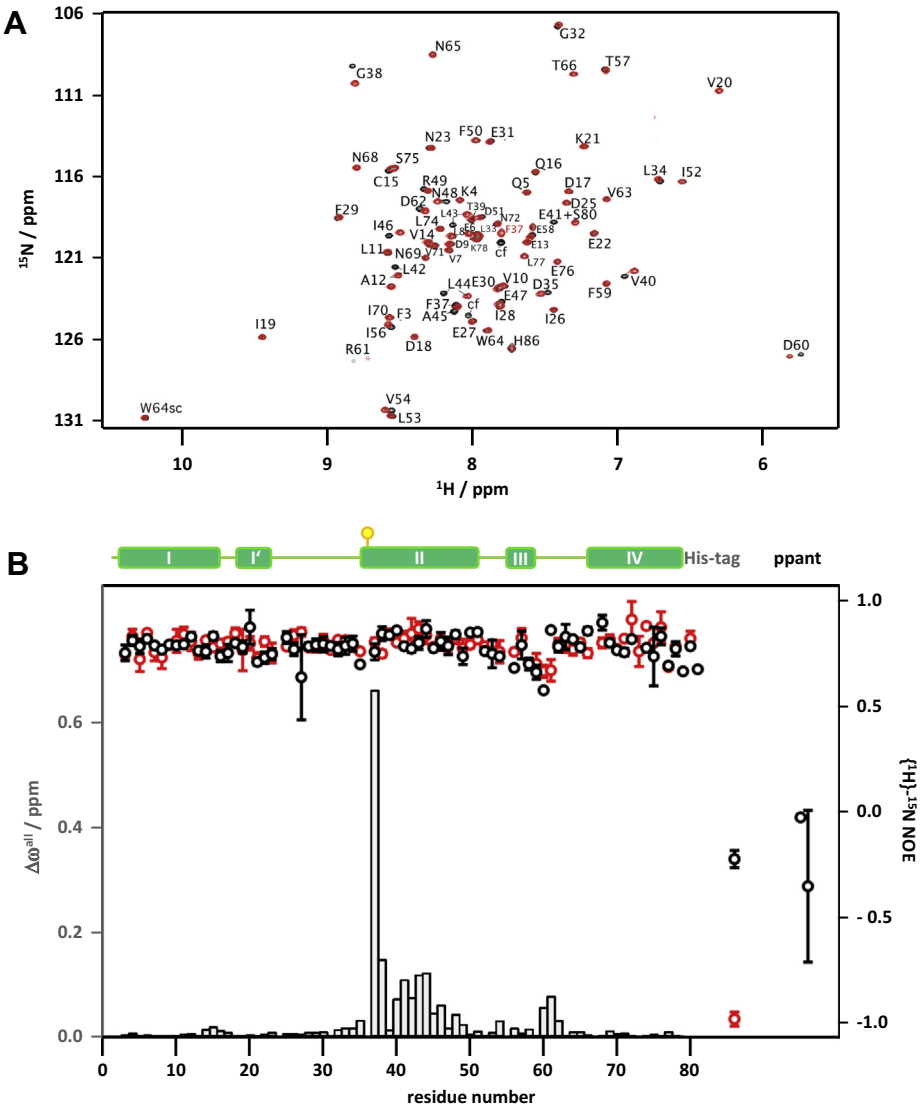

Fig. 3. ^{1}H-^{15}N TROSY HSQC NMR spectroscopy demonstrates the structural equivalence of *apo*- and *holo*-DltC in solution. (A) No major changes in chemical shifts indicative of large scale structural rearrangements are seen upon superposition of spectra for *apo*- and *holo*-DtlC (red and black, respectively). Resonances could not be assigned to Ser/Ala36, the site of ppant attachment, which has also been observed for ACP from *E. coli* [45]. On the other hand, cross peaks corresponding to the ppant cofactor (*cf*) were observed, confirming its presence in the *holo*-DltC sample. Note the single peak for the indole nitrogen of Trp64 (W64sc) in both spectra. (B) Chemical shift deviation (grey bars; left ordinate) plotted as a function of residue number (average chemical shift deviation $\Delta\omega^{all} \sim 0.017$ ppm), together with a schematic representation of secondary structure element demarcations on the top. The largest shift is seen for the backbone amide of Phe37 in the immediate vicinity of the ppant attachment site. Overlaid are the spin-relaxation data for *apo*- and *holo*-DltC (red and black circles, respectively; right ordinate) derived from steady-state {^{1}H}-^{15}N heteronuclear NOE experiments. The two data points to the far right of the plot represent relaxation data for the NH groups of the ppant moiety.

on the picosecond–nanosecond timescale. It cannot however be ruled out that the phosphoester bond of crystallized *holo*-DltC has been hydrolyzed, as species corresponding to phosphorylated DltC (due to the loss of a pantetheine moiety) could be observed in ESI-MS measurements (Supplementary Fig. 2).

In *holo*-DltC crystal form II on the other hand, well defined electron density is observed for the entire cofactor (Fig. 2D). The position of the pantetheinyl side chain, which folds back along the surface of the protein, is very probably strongly influenced by formation of a disulfide bond to a symmetry-related molecule. A similar disulfide linkage between symmetry molecules has been observed in the crystal structure of the ACP from *Plasmodium falciparum* (*Pf*ACP) [42]. In keeping with the notion that such disulfide-linked carrier protein dimers are due to oxidation during protein preparation [43,44], the protein–protein interface in *holo*-DltC crystal form II is completely different to that in *Pf*ACP. In both proteins, the side chain of Ser36 is in the *gauche* (+) conformation, while all other ppant torsion angles differ. To accommodate the orientation of the ppant arm in *holo*-DltC crystal form II, the side chain of Phe37 rotates away from its position in *apo*-DltC and *holo*-DltC crystal form I, although this is more likely due to the observed crystal packing environment than to the presence of the cofactor. The overall structure of *holo*-DltC in crystal form II is similar to those in the other crystals, with rmsd Cα positions of 0.41 Å (*apo*-DltC) and 0.63 Å/0.65 Å (*holo*-DltC crystal form I, molecules A and B).

As no major differences in structure could be identified within the different crystal forms, NMR spectroscopy was performed to investigate the behaviour of DltC in solution. The resulting ^{1}H-^{15}N TROSY HSQC spectra (Fig. 3) revealed an equivalent set of cross peaks for *apo*- and *holo*-DltC, with the appearance of two additional resonances (due to the two ppant amide moieties) in the *holo*-DltC spectrum confirming the integrity of the cofactor. Analysis of the weighted chemical shift deviations demonstrates that only resonances in the immediate neighbourhood of the ppant attachment site are affected by cofactor modification. The largest shift is seen for the backbone amide of Phe37, the residue immediately following the reactive site Ser36, followed by those of the ensuing helix II (Gly38-Ile46) and the sequence Asp60-Asp62. The latter includes Arg61, whose side chain guanidinium moiety is directed towards the cofactor phosphate. Thus upon cofactor attachment, DltC behaves as other carrier proteins in solution [13,19,45]. Analysis of backbone dynamics using $\{^{1}H\}$-^{15}N heteronuclear NOE data reveal very similar fluctuations of *apo*- and *holo*-DltC on the picosecond–nanosecond time scales (Fig. 3B). Finally, ^{15}N R_2 relaxation dispersion data show no sign of exchange dynamics to an alternative state (>0.5%) in the millisecond time scale (data not shown).

The data reported here lead us to conclude that DltC does not adopt cofactor-dependent alternative conformations in solution. This is in accordance with other recent studies [19–22] that find no evidence for the large scale conformational changes reported for the TycC3-PCP [8], suggesting that it is time to reconsider the role of carrier protein plasticity in natural product biosynthesis.

Acknowledgements

We thank Dr. Christian Ihling (Institut für Pharmazie, Martin-Luther-Universität Halle-Wittenberg) for collection and analysis of the ESI-MS data. Diffraction data for the *apo*-DltC crystals and *holo*-DltC crystal form I were measured at the Protein Structure Factory beamline BL14.1 of BESSY and the Free University Berlin. This work was supported in part by the DFG Graduiertenkolleg 1026 "Conformational transitions in macromolecular interactions" to M.T.S. and J.B.

Appendix A. Supplementary data

Supplementary data associated with this article can be found, in the online version, at http://dx.doi.org/10.1016/j.febslet.2015.07.008.

References

[1] Neuhaus, F.C. and Baddiley, J. (2003) A continuum of anionic charge: structures and functions of D-alanyl-teichoic acids in gram-positive bacteria. Microbiol. Mol. Biol. Rev. 67, 686–723.
[2] Swoboda, J.G., Campbell, J., Meredith, T.C. and Walker, S. (2010) Wall teichoic acid function, biosynthesis, and inhibition. ChemBioChem 11, 35–45.
[3] Peschel, A., Otto, M., Jack, R.W., Kalbacher, H., Jung, G. and Gotz, F. (1999) Inactivation of the dlt operon in Staphylococcus aureus confers sensitivity to defensins, protegrins, and other antimicrobial peptides. J. Biol. Chem. 274, 8405–8410.
[4] Collins, L.V., Kristian, S.A., Weidenmaier, C., Faigle, M., Van Kessel, K.P., Van Strijp, J.A., Gotz, F., Neumeister, B. and Peschel, A. (2002) Staphylococcus aureus strains lacking D-alanine modifications of teichoic acids are highly susceptible to human neutrophil killing and are virulence attenuated in mice. J. Infect. Dis. 186, 214–219.
[5] Perego, M., Glaser, P., Minutello, A., Strauch, M.A., Leopold, K. and Fischer, W. (1995) Incorporation of D-alanine into lipoteichoic acid and wall teichoic-acid in *bacillus subtilis* – identification of genes and regulation. J. Biol. Chem. 270, 15598–15606.
[6] Volkman, B.F., Zhang, Q.Y., Debabov, D.V., Rivera, E., Kresheck, G.C. and Neuhaus, F.C. (2001) Biosynthesis of D-alanyl-lipoteichoic acid: the tertiary structure of apo-D-alanyl carrier protein. Biochemistry 40, 7964–7972.
[7] Weissman, K.J. and Muller, R. (2008) Protein-protein interactions in multienzyme megasynthetases. ChemBioChem 9, 826–848.
[8] Koglin, A., Mofid, M.R., Lohr, F., Schafer, B., Rogov, V.V., Blum, M.M., Mittag, T., Marahiel, M.A., Bernhard, F. and Dotsch, V. (2006) Conformational switches modulate protein interactions in peptide antibiotic synthetases. Science 312, 273–276.
[9] Koglin, A., Lohr, F., Bernhard, F., Rogov, V.V., Frueh, D.P., Strieter, E.R., Mofid, M.R., Guntert, P., Wagner, G., Walsh, C.T., Marahiel, M.A. and Dotsch, V. (2008) Structural basis for the selectivity of the external thioesterase of the surfactin synthetase. Nature 454. 907-U68.
[10] Rock, C.O. and Garwin, J.L. (1979) Preparative enzymatic-synthesis and hydrophobic chromatography of acyl–acyl carrier protein. J. Biol. Chem. 254, 7123–7128.
[11] Roujeinikova, A., Baldock, C., Simon, W.J., Gilroy, J., Baker, P.J., Stuitje, A.R., Rice, D.W., Slabas, A.R. and Rafferty, J.B. (2002) X-ray crystallographic studies on butyryl-ACP reveal flexibility of the structure around a putative acyl chain binding site. Structure 10, 825–835.
[12] Zornetzer, G.A., Fox, B.G. and Markley, J.L. (2006) Solution structures of spinach acyl carrier protein with decanoate and stearate. Biochemistry 45, 5217–5227.
[13] Evans, S.E., Williams, C., Arthur, C.J., Burston, S.G., Simpson, T.J., Crosby, J. and Crump, M.P. (2008) An ACP structural switch: conformational differences between the Apo and Holo forms of the actinorhodin polyketide synthase acyl carrier protein. ChemBioChem 9, 2424–2432.
[14] Crosby, J. and Crump, M.P. (2012) The structural role of the carrier protein–active controller or passive carrier. Nat. Prod. Rep. 29, 1111–1137.
[15] Weber, T., Baumgartner, R., Renner, C., Marahiel, M.A. and Holak, T.A. (2000) Solution structure of PCP, a prototype for the peptidyl carrier domains of modular peptide synthetases. Struct. Fold. Des. 8, 407–418.
[16] Goodrich, A.C. and Frueh, D.P. (2015) A nuclear magnetic resonance method for probing molecular influences of substrate loading in nonribosomal peptide synthetase carrier proteins. Biochemistry 54, 1154–1156.
[17] Drake, E.J., Nicolai, D.A. and Gulick, A.M. (2006) Structure of the EntB multidomain nonribosomal peptide synthetase and functional analysis of its interaction with the EntE adenylation domain. Chem. Biol. 13, 409–419.
[18] Sundlov, J.A., Shi, C., Wilson, D.J., Aldrich, C.C. and Gulick, A.M. (2012) Structural and functional investigation of the intermolecular interaction between NRPS adenylation and carrier protein domains. Chem. Biol. 19, 188–198.
[19] Haslinger, K., Redfield, C. and Cryle, M.J. (2015) Structure of the terminal PCP domain of the non-ribosomal peptide synthetase in teicoplanin biosynthesis. Proteins 83, 711–721.
[20] Allen, C.L. and Gulick, A.M. (2014) Structural and bioinformatic characterization of an Acinetobacter baumannii type II carrier protein. Acta Crystallogr. D Biol. Crystallogr. 70, 1718–1725.
[21] Lohman, J.R., Ma, M., Cuff, M.E., Bigelow, L., Bearden, J., Babnigg, G., Joachimiak, A., Phillips Jr., G.N. and Shen, B. (2014) The crystal structure of BlmI as a model for nonribosomal peptide synthetase peptidyl carrier proteins. Proteins 82, 1210–1218.
[22] Tufar, P., Rahighi, S., Kraas, F.I., Kirchner, D.K., Lohr, F., Henrich, E., Kopke, J., Dikic, I., Guntert, P., Marahiel, M.A. and Dotsch, V. (2014) Crystal structure of a PCP/Sfp complex reveals the structural basis for carrier protein posttranslational modification. Chem. Biol. 21, 552–562.

[23] Linne, U., Schafer, A., Stubbs, M.T. and Marahiel, M.A. (2007) Aminoacyl-coenzyme A synthesis catalyzed by adenylation domains. FEBS Lett. 581, 905–910.
[24] Yonus, H., Neumann, P., Zimmermann, S., May, J.J., Marahiel, M.A. and Stubbs, M.T. (2008) Crystal structure of DltA: implications for the reaction mechanism of non-ribosomal peptide synthetase adenylation domains. J. Biol. Chem. 283, 32484–32491.
[25] May, J.J., Finking, R., Wiegeshoff, F., Weber, T.T., Bandur, N., Koert, U. and Marahiel, M.A. (2005) Inhibition of the D-alanine: D-alanyl carrier protein ligase from *Bacillus subtilis* increases the bacterium's susceptibility to antibiotics that target the cell wall. FEBS J. 272, 2993–3003.
[26] Kabsch, W. (2010) Xds. Acta Crystallogr. Section D-Biol. Crystallogr. 66, 125–132.
[27] Winn, M.D., Ballard, C.C., Cowtan, K.D., Dodson, E.J., Emsley, P., Evans, P.R., Keegan, R.M., Krissinel, E.B., Leslie, A.G., McCoy, A., McNicholas, S.J., Murshudov, G.N., Pannu, N.S., Potterton, E.A., Powell, H.R., Read, R.J., Vagin, A. and Wilson, K.S. (2011) Overview of the CCP4 suite and current developments. Acta Crystallogr. D Biol. Crystallogr. 67, 235–242.
[28] Sheldrick, G.M. (2008) A short history of SHELX. Acta Crystallogr. Section A 64, 112–122.
[29] Pape, T. and Schneider, T.R. (2004) HKL2MAP: a graphical user interface for macromolecular phasing with SHELX programs. J. Appl. Crystallogr. 37, 843–844.
[30] Langer, G., Cohen, S.X., Lamzin, V.S. and Perrakis, A. (2008) Automated macromolecular model building for X-ray crystallography using ARP/wARP version 7. Nat. Protoc. 3, 1171–1179.
[31] Emsley, P., Lohkamp, B., Scott, W.G. and Cowtan, K. (2010) Features and development of Coot. Acta Crystallogr. D Biol. Crystallogr. 66, 486–501.
[32] Afonine, P.V., Grosse-Kunstleve, R.W., Echols, N., Headd, J.J., Moriarty, N.W., Mustyakimov, M., Terwilliger, T.C., Urzhumtsev, A., Zwart, P.H. and Adams, P.D. (2012) Towards automated crystallographic structure refinement with phenix.refine. Acta Crystallogr. D Biol. Crystallogr. 68, 352–367.
[33] Mccoy, A.J., Grosse-Kunstleve, R.W., Adams, P.D., Winn, M.D., Storoni, L.C. and Read, R.J. (2007) Phaser crystallographic software. J. Appl. Crystallogr. 40, 658–674.
[34] Grzesiek, S., Stahl, S.J., Wingfield, P.T. and Bax, A. (1996) The CD4 determinant for downregulation by HIV-1 Nef directly binds to Nef. Mapping of the Nef binding surface by NMR. Biochemistry 35, 10256–10261.
[35] Tollinger, M., Skrynnikov, N.R., Mulder, F.A., Forman-Kay, J.D. and Kay, L.E. (2001) Slow dynamics in folded and unfolded states of an SH3 domain. J. Am. Chem. Soc. 123, 11341–11352.
[36] Delaglio, F., Grzesiek, S., Vuister, G.W., Zhu, G., Pfeifer, J. and Bax, A. (1995) NMRPipe: a multidimensional spectral processing system based on UNIX pipes. J. Biomol. NMR 6, 277–293.
[37] Johnson, B.A. and Blevins, R.A. (1994) NMR View: a computer program for the visualization and analysis of NMR data. J. Biomol. NMR 4, 603–614.
[38] Richardson, J.S. and Richardson, D.C. (1988) Amino acid preferences for specific locations at the ends of alpha helices. Science 240, 1648–1652.
[39] Parris, K.D., Lin, L., Tam, A., Mathew, R., Hixon, J., Stahl, M., Fritz, C.C., Seehra, J. and Somers, W.S. (2000) Crystal structures of substrate binding to *Bacillus subtilis* holo-(acyl carrier protein) synthase reveal a novel trimeric arrangement of molecules resulting in three active sites. Struct. Fold. Des. 8, 883–895.
[40] Mitchell, C.A., Shi, C., Aldrich, C.C. and Gulick, A.M. (2012) Structure of PA1221, a nonribosomal peptide synthetase containing adenylation and peptidyl carrier protein domains. Biochemistry 51, 3252–3263.
[41] Flocco, M.M. and Mowbray, S.L. (1994) Planar stacking interactions of arginine and aromatic side-chains in proteins. J. Mol. Biol. 235, 709–717.
[42] Gallagher, J.R. and Prigge, S.T. (2010) Plasmodium falciparum acyl carrier protein crystal structures in disulfide-linked and reduced states and their prevalence during blood stage growth. Proteins Struct. Funct. Bioinform. 78, 575–588.
[43] De Lay, N.R. and Cronan, J.E. (2007) In vivo functional analyses of the type II acyl carrier proteins of fatty acid biosynthesis. J. Biol. Chem. 282, 20319–20328.
[44] Rock, C.O., Cronan Jr., J.E. and Armitage, I.M. (1981) Molecular properties of acyl carrier protein derivatives. J. Biol. Chem. 256, 2669–2674.
[45] Kim, Y., Kovrigin, E.L. and Eletr, Z. (2006) NMR studies of *Escherichia coli* acyl carrier protein: dynamic and structural differences of the apo- and holo-forms. Biochem. Biophys. Res. Commun. 341, 776–783.